J Appl Electrochem (2013) 43:217–225
DOI 10.1007/s10800-012-0485-2

ORIGINAL PAPER

Investigation and optimization of photocurrent transient measurements on nano-TiO_2

F. Spadavecchia · S. Ardizzone · G. Cappelletti · L. Falciola · M. Ceotto · D. Lotti

Received: 16 July 2012 / Accepted: 21 September 2012 / Published online: 2 October 2012

Abstract Chronoamperometry with chopped light has been applied to commercial and homemade TiO_2 nanopowders, both doped and undoped, to gain information on the charge recombination processes which take place in the oxide and affect its photocatalytic performance. The photocurrent transients can be attributed to photoinduced electron–hole separation, trapping, recombination, and scavenging. In order to evaluate what mainly affects the shape of the transients and the transient time constants (τ) which can be derived, the type and concentration of the electrolyte, the irradiation source (UV or visible light), and the presence of a hole acceptor (oxalate) were varied. The reproducibility of quantitative measurements was best when an inert electrolyte ($NaClO_4$) has been employed under an N_2-saturated atmosphere. Under these conditions, both Pr-TiO_2 and N-TiO_2 samples show a definitely higher τ than the undoped oxide, which indicates a slower recombination kinetics, both under UV and visible irradiation. Therefore, these are promising as photocatalysts.

Keywords Photocurrent · Nano-TiO_2 · Recombination · Transient time constant · Electrolyte · Irradiation source

1 Introduction

High surface area metal oxide electrodes, with nanoporous morphology, are currently of great interest because of their unprecedented properties, as TiO_2 has shown over the last decades and even increasingly in the last years. Specifically, many recent innovations in photoelectrochemical solar energy conversion exploit porous nanocrystalline films [1–3] which are usually composed of a three-dimensional network of interconnected nano-sized particles and exhibit many unique optical and electrical properties in comparison to planar single-crystal or non-porous polycrystalline films.

Nanostructured semiconductor thin films exhibit a large strength in various fields such as photovoltaics, photocatalysis, sensors, and optoelectronics [4–7]. As a consequence, it is of paramount importance to explore the behavior of the semiconductor thin films in contact with an electrolyte [8] and to understand phenomena related to charge transport and recombination.

Several mechanisms for electron transport have been suggested, e.g., a hopping type mechanism [9, 10] and the possibility of tunneling through a potential barrier between the particles [11, 12]. If no macroscopic electric field exists in the system (nanometric particles), both processes may be considered as a random motion between equivalent sites and diffusion governs electron transport.

Experimental measurements as well as computer simulations have been carried out extensively to study the electron diffusion coefficient. It has been found that this parameter is not only related to the structure of the mesoporous film [13] and to the "necking" of neighboring nanoparticles [14, 15] but also to the composition of the electrolyte via an ambipolar diffusion mechanism [16] and to the incident light intensity, as first reported by Cao et al. [17]. A great variety of experimental methods have been used to study the electron transport processes in mesoporous TiO_2 films, ranging from small-amplitude modulation methods such as intensity-modulated photocurrent spectroscopy [18–20] and transient photocurrent

F. Spadavecchia (✉) · S. Ardizzone · G. Cappelletti · L. Falciola · M. Ceotto · D. Lotti
Dipartimento di Chimica, Università degli Studi di Milano, Via Golgi 19, 20133 Milan, Italy
e-mail: francesca.spadavecchia@unimi.it

measurements [16, 21] to electrical impedance spectroscopy applied to both mesoporous TiO_2 electrodes [22] as well as to complete dye-sensitized solar cells [23]. Charge transport measurements have been also conducted in open-circuit conditions by a transient voltage rise method [24]. DC conductivity measurements of mesoporous TiO_2 electrodes have been performed in redox inactive electrolytes [25], while conductivity measurements by microwave absorption [26] and terahertz spectroscopy [27] have been performed in the absence of electrolyte. Experimental results have demonstrated that the measured (effective) diffusion coefficient is closely related to the quasi-Fermi level in the mesoporous TiO_2 [22, 23].

Because of their successful use in combined studies on dye-sensitized solar cells, photocurrent transients following the injection of electrons from the excited state of the dye into the conduction band of the semiconductor have been quite widely investigated in literature, as a means to probe the working electrode and to understand the factors which determine the final operative short circuit current of the cell. In these cases and when the photocurrent is recorded as a function of the applied potential, the system under study is composed not by the bare TiO_2 electrode alone: this latter is either sensitized by the dye or measurements are directly performed on the assembled solar cell [28–30].

In this work, we want to test the bare (doped-)TiO_2 electrode, without dye, keeping the system as simple as possible in order to characterize the charge recombination behavior of our home-made samples by a useful traditional photoelectrochemical technique which is very rarely used for this specific purpose.

Nevertheless, other literature works present chopped light amperometric measurements on nano-TiO_2 electrodes [31, 32] or other inorganic semiconductor devices [33] under potentiostatic conditions in aqueous electrolytes. Such experimental data allow to qualitatively judge the photocurrent and eventually compare it with the dark current. Alternatively, polarization curves on irradiated TiO_2 layers were measured by Waldner et al. in various electrolytes, namely sodium hydroxide, sulfuric acid, oxalic acid, and potassium oxalate [34, 35]. The shape of such curves was interpreted in terms of response time to irradiation and photocurrent depletion. Besides, the photocurrent developed following a ns laser pulse (bandgap excitation) has been monitored under steady-state conditions in a certain number of literature studies [17, 29], in some cases to give a merely qualitative description of charge carrier separation and charge transport in nanocrystalline porous TiO_2 electrodes. Then, electron migration in nanostructured anatase TiO_2 films by intensity-modulated photocurrent spectroscopy was investigated by Goossens et al. [36], who described the transport of electrons by a macroscopic diffusion model.

However, very few papers deal with chronoamperometric measurements and the consequent evaluation of the transient time constant (τ) making use of this characterization mainly to investigate the electronic properties of the tested samples and also to judge their photoactivity.

Indeed, we propose the use of such a tool as a helpful prescreen of semiconductor oxides synthesized in powdery form. No literature examples exist with this specific aim. We offer a method which turns out to be useful for any type of nano-TiO_2, starting from both powders and films. As most of metal or non-metal doped titania samples are obtained by wet methods, like the sol–gel route, they are usually produced and used in photocatalytic applications as powders. Then, their deposition as suitable electrodes for chronoamperometric tests is not trivial at all.

Thus, we decided to present a comprehensive evaluation of the optimal conditions that allow reproducible quantitative photocurrent measurements on thin TiO_2 films by varying different experimental parameters such as the type of electrolyte, the illumination source, and the presence of a hole acceptor.

Since the efficient utilization of the solar spectrum is one of the important subjects for improving the future generation of TiO_2-based photocatalysts, also metal and non-metal-doped titania have been analyzed by chopped light chronoamperometry.

2 Experimental

2.1 Preparation of TiO_2 powders and films

A sol–gel method from titanium isopropoxide as precursor was used to synthesize TiO_2 nanopowders following a procedure previously reported [37]. N- and Pr-doped TiO_2 samples ("T_N" and "T_Pr", respectively) were obtained by adding, at the initial stage of the sol–gel, triethylamine [37] and praseodymium(III) nitrate hexahydrate in basic and acidic pH, respectively, keeping the same synthetic route used for the undoped sample ("T"). The stoichiometric dopant/Ti nominal molar ratio was set equal to 0.1 for N and 0.001 for Pr. These values are among the most used in literature and lead to a pretty similar final amount of dopant in the TiO_2 lattice since most of the nitrogen is lost during calcination (by XPS analysis the final N/Ti ratio is one or two orders of magnitude lower than the starting values [37]).

TiO_2 thin films were prepared by spin coating a 2-propanol suspension of the oxide powder with a Spin150 spin-coater (SPS, ATP GmbH) onto flourine-doped tin oxide conducting glass (Aldrich, 2.3-mm thick, $\sim$7 Ω/sq surface resistivity). The suspension was drop cast on the substrate and spun at 2,000 rpm for 20 s using a scotch tape as a

frame to have an active area of 3 cm^2. The deposition was repeated for eight layers. The as-prepared films were finally sintered at 400 °C in air for 1 h.

2.2 Material characterization

For the characterization of the undoped and N- or Pr-doped TiO_2 samples, diffuse-reflectance spectra of the powders were measured on a UV–Vis spectrophotometer (Perkin-Elmer, Lambda 35) equipped with a diffuse reflectance accessory [37].

HR-TEM technique has been resorted to JEOL 3010 TEM microscope, 300 kV acceleration, LaB6 filament, Cu copper grids coated with "holey" carbon film.

To gain information on the theoretical density of states (DOS) of the samples, periodic three-dimensional DFT calculations were carried out using the VASP 4.6 code [38] with the projector augmented wave method [39], as previously reported [40, 41]. Here, the U parameter that provides an on-site correction to describe systems with localized d and f electrons was set equal to 3.3 eV for Ti.

2.3 Photocurrent setup

The photocurrent developed by irradiating the photoanode (TiO_2) with either UV or visible light [42] was recorded by a microIII Autolab potentiostat/galvanostat (EcoChemie, The Netherlands). The photoelectrochemical cell was a three-compartment one with two counter electrodes, both consisting in a Pt wire parallel to the working electrode, a saturated calomel electrode as reference, a Luggin capillary to minimize the ohmic drop and a TiO_2 film located in the middle of the cell as working electrode. Different aqueous electrolytes were used with spontaneous pH: NaCl, NaOH, and $NaClO_4$ at the concentration of 0.1 M (selected as the best one). Acidic conditions were avoided on the grounds of literature evidences [43, 44]. Chuang et al. [43] reported that even though a slightly higher photocurrent was observed in the acidic electrolyte (0.1 M HNO_3) because the mobility of H^+ ions was much higher than that of OH^- ions, under irradiation of both UV and visible light in 0.1 M HNO_3, the utilization of doped TiO_2 nanoparticle thin films as a photoelectrodes became unsuitable. Wang et al. [44] in their study on a commercial titania sample found out that the charge decreases with the proton concentration in the solution.

Besides these, the influence of a hole acceptor (10^{-3} M aq. oxalate) in the presence of the best selected inert electrolyte ($NaClO_4$) was studied. The photoanode was alternatively exposed to dark and light, from the electrode–electrolyte side, using two irradiation sources: UV light generated by a 500-W UV halogen lamp (Jelosil HG 500, iron halides) or visible light by a LOT-Oriel lamp (Lamp Housing LSH302), emitting in the range 315–400 nm and 400–950 nm and presenting an effective power of 150 and 205 mW (measured by Thorlabs S314C at a distance of 15 cm), respectively.

All the measurements have been carried out in N_2 atmosphere after degassing the cell with nitrogen flow for at least 10 min. Stirring and N_2 bubbling are avoided during the tests to eliminate any noise in the signal.

Preliminary linear sweep voltammetries (LSV) have been recorded in the same experimental conditions at a scan rate of 50 mV s^{-1} to evaluate the potential at which the photocurrent is constant to be chosen as working potential for the chronoamperometric tests. The photocurrent-time behavior under constant electrode polarization was then obtained with hand-chopped light. Before recording the transient, the applied potential was kept constant in the dark for 600 s to establish dark current equilibrium [42] and nitrogen was flown into the cell. Afterward, the electrodes were exposed to light for 200 s. During this time, the current transient was recorded. A 100-s dark exposition followed after a new exposure to light. The dark/light alternation was repeated for at least 6 times to obtain reproducible transient patterns.

3 Results and discussion

For an n-type semiconductor like defective nano-TiO_2, illumination with above-bandgap light promotes and accumulates electrons in the conduction band of the nanostructured film with a fraction of them being stored into deep surface states [36].

Nanometer-sized particles are generally too small to sustain significant electric fields so that transport of electrons (majority carriers) in the network of particles is expected to be dominated by a gradient in the chemical potential of the electrons (diffusion) rather than by an electrical potential gradient (drift) [17].

The photocurrent response of the titania electrodes was first evaluated by linear sweep voltammetry to examine charge-carrier characteristics at the semiconductor/electrolyte interface and to evaluate the optimized potential at which the photocurrent was the highest or remained constant. LSV in a dark room showed minute current in the 10^{-7}–10^{-6} A cm^{-2} range from 0 V up to approximately +1.0 V (SCE). LSV performed by irradiating the system with UV or visible light, starting from negative potentials, presented a very similar shape to that obtained in the dark, just shifted to higher current in the positive potential range, in the presence of an inert electrolyte (0.1 M $NaClO_4$), as can be appreciated in Fig. 1a. In the case of other electrolytes (NaCl, NaOH), the photocurrent increased incessantly moving to positive potentials, not saturating

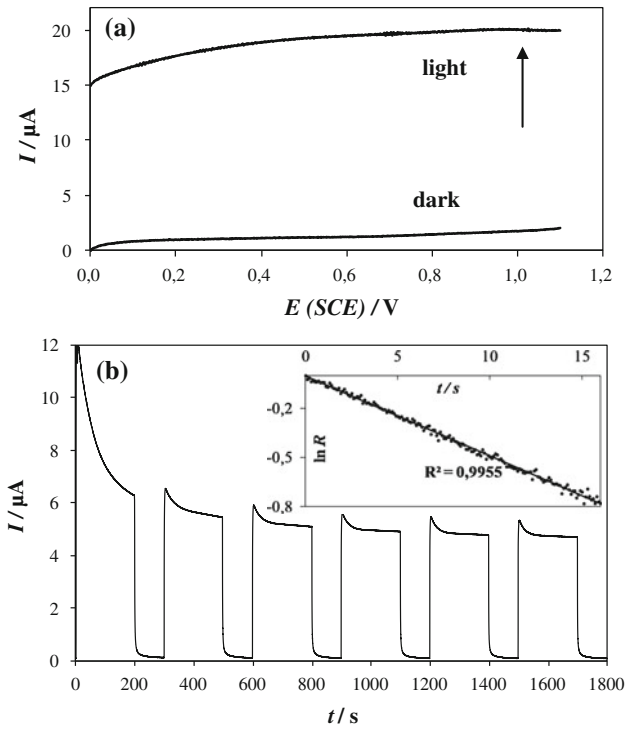

Fig. 1 Linear sweep voltammetries (LSV) recorded for a selected sample (T) under dark and illumination before performing the chronoamperometric test (**a**); the arrow indicates the potential chosen for the chronoamperometric measurements. Typical example of photocurrent transients (sample T) with the normalized plot of current–time dependence in *inset* (**b**)

completely below 1.0 V: an optimized depletion layer was not fully formed. The increase of photocurrent enlightened the effective charge separation because the recombination of photoinduced electron–hole pairs was inhibited by the increase of positive potential.

According to Poznyak et al. [45], in the case of nanostructured electrodes, the photocurrent is almost independent of potential in a rather wide range of potential values and starts to change sharply just near the onset potential (i.e.,. flat band potential/quasi-Fermi level under irradiation). Thus, we decided to record the chronoamperometry measurements at +1.0 V (SCE), except for the experiments conducted in aqueous NaOH; in such cases, the potential was set at + 0.4 V (in basic media the flat band potential is shifted because of the Nernstian dependence with pH).

The photocurrent–time response of the semiconductor electrode was evaluated by chronoamperometry under a constant potential using hand chopped light. The typical output of the experiment, in the case of a proper inert electrolyte, is shown in Fig. 1b. The immediate photoresponse (I_{in}) consists in an anodic spike caused by the separation of photogenerated electron–hole pairs at the semiconductor/electrolyte interface, followed by an exponential decrease of the photocurrent with time until a stationary value is reached (I_{st}). By defining the ratio R as

$$R = \frac{I_t - I_{st}}{I_{in} - I_{st}} \quad (1)$$

in which I_t is the current at time t, the photocurrent transient can be described by the following kinetic equation:

$$R = e^{-\frac{t}{\tau}} \quad (2)$$

in which τ is the transient time constant. Thus, the slope of the ln(R) *vs* time plot (inset of Fig. 1b) is the reciprocal of τ, which is related to the mechanism of electron transport and gives indications about the time for charge recombination processes in the film. The higher the transient time constant, the more inhibited the recombination processes are. In this work, the numerical value of τ is extracted by at least three transient peaks (from 700 to 1,550 s after switching the lamp on), and an average value is given for each sample. The choice of the same transients for quantitative elaborations allows to make a reasonable comparison among all samples. In the literature, no clear details on the data point used to extract the transient time constants are provided. Dholam et al. [46] adopted transient time constants from chronoamperometric measurements on the time scale of tens/hundred of seconds to exploit the recombination behavior of multilayer Cr-doped TiO_2. However, in the normalized plot of current–time dependence, the choice of the time range for quantitative extrapolation is not straightforward and varied for different samples. Moreover, it has been found that some authors compare the photocurrent absolute intensity of different systems without taking into account every intrinsic or experimental differences that lie in the home-made semiconductor electrodes: Zhang et al. [33] showed the photocurrent transient generated under chopped UV irradiation for ZnO nanowires, multiwalled carbon nanotubes (MWCNTs), and a composite system in which the nanowires were adhesively grown on the MWCNTs; they commented on the very weak photoresponse of the MWCNTs and made comparison on the numerical values obtained for each device though the thickness of each deposited system was not the same.

The linear behavior observed for all our tested materials indicates that the decay mechanism is only due to surface recombination leading to a first-order kinetics in electron surface concentration, as found by Dholam et al. [46] for Cr-TiO_2 and asserted by Tafalla and coauthors [47].

All measurements have been carried out in nitrogen atmosphere allowing the achievement of more reproducible data. Thus, the cell was deareated avoiding the presence of oxygen which plays the role of electron acceptor. Byrne et al. [31] also reported that when oxygen is present in the anode compartment, the photocurrent response is smaller than when oxygen is absent from both compartments or present

only in the cathodic one. Moreover, the quenching of anodic photocurrent, due to the presence of oxygen in the anode, is said to occur even at positive potentials up to 1.0 V, as previously observed also by Rensmo et al. and Hagfeldt et al. [42, 48]. They hypothesized that since the conduction band electrons at the surface of a relatively thick TiO_2 film have a finite distance to travel before reaching the substrate, adsorbed oxygen actively scavenges such electrons from the oxide surface preventing them from reaching the substrate and a reduction in the anodic current is observed.

Since semiconductor particles in a nanostructured film are surrounded by electrolyte and photoelectrons may be trapped by an electron acceptor in the electrolyte during the time they need to reach the back contact, the probability of such process would grow as the distance from the substrate increases. Therefore, the thickness of the films has been kept nearly constant (about 1–2 μm, measured by DekTak 150 step-profilometer) by depositing the same amount of TiO_2 suspension (8 layers).

3.1 Role of the electrolyte and of a hole acceptor

Photogenerated electrons and holes are quickly trapped at surface states in nanocrystalline TiO_2 films [45]; in this way, they can participate independently in surface reduction and oxidation processes involving redox-active species in solution.

The response of the electrode in the presence of different electrolytes (see Sect. 2) has been deeply analyzed with the aim of comparing the most used systems in the literature.

Figure 2 displays the chronoamperometric tests registered when the titania electrode is in contact with NaCl or NaOH. It is possible to observe that a minor photocurrent decay is noticeable in the latter case and a final rise without a satisfactory steady-state photocurrent appears in the transient obtained with NaCl, as also reported by Xiao et al. [49] in the case of TiO_2/Ti nanotube electrodes. As a hole acceptor, chloride ions can lead to deviations in transient shapes due to the modification of the photoanode surface according to the following adsorption phenomena [49]:

$$TiO_2 - h^+ + Cl^- \rightarrow TiO_2 - Cl_{ads} \quad (3)$$

Moreover, because of this ability in scavenging holes, chloride ions may promote the separation of electron–hole pairs. Then, at chloride concentrations lower than 0.1 M, the electron/hole pairs generated at a steady state rate can recombine preferentially since chloride ions are weakly adsorbed onto the semiconductor electrode. However, at higher concentrations of chloride, it is likely that the adsorption effect would predominate, avoiding charge recombination, as Zanoni et al. [50] suggested. In our work, this fact results in transients with the same order of photocurrent values as those obtained with other electrolytes and a disadvantageous profile of the photocurrent decay.

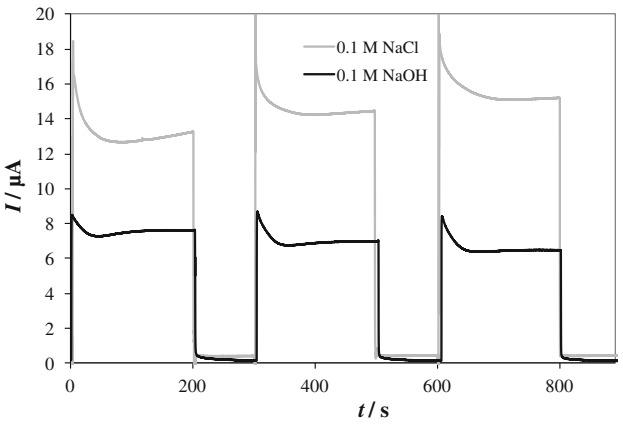

Fig. 2 Photocurrent transients recorded for the undoped oxide (sample T) in the presence of two different aqueous electrolytes (0.1 M NaCl and 0.1 M NaOH) with the same experimental conditions

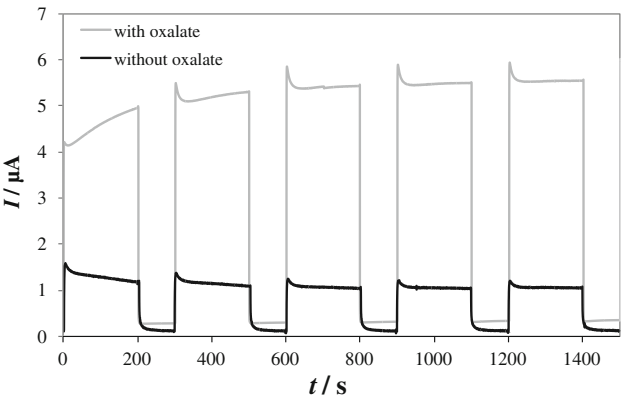

Fig. 3 Photocurrent transients recorded for the undoped oxide (sample T) with or without a hole acceptor (oxalate) using aqueous 0.1 M $NaClO_4$ as electrolyte

Thus, on the basis of the present results, 0.1 M $NaClO_4$ is chosen as the best inert electrolyte.

In the literature, the experimental setup is sometimes more complex than ours and a quite common way of performing such measurements is that of using a hole acceptor other than the bare electrolyte. When adding such species, such as oxalate, the response is significantly enhanced (Fig. 3). This can be ascribed to the fact that some holes are captured by oxalate and a higher amount of electrons are collected at the counter electrode. Byrne et al. [31] explained this effect by the so-called current doubling:

$$^{-}OOC - COO^{-} + h^+ \rightarrow COO^{-} + CO_2 \rightarrow 2CO_2 + e^- \quad (4)$$

However, adding in solution such substances which oxidize irreversibly at TiO_2 not only results in a significant increase in the quantum efficiency of the photoelectrochemical process but also changes the photocurrent spectrum shape in the case of nanostructured TiO_2 electrodes, according to the study of Poznyak et al. [45] They found some difficulties in explaining

Table 1 Morphological (BET surface area and total pore volume), structural (anatase and brookite wt% and anatase domain size), and optical (apparent band gap) features for all samples

Sample	Dopant/Ti initial molar ratio	S_{BET} ($m^2\ g^{-1}$)	Pore volume (mL g^{-1})	d^A_{101} (nm)	% anatase	% brookite	Apparent band gap (eV)
T	–	170	0.31	7	70	30	3.21
T_N	0.1	120	0.10	7	77	23	2.98
T_Pr	0.001	95	0.15	12	61	39	3.01

the influence of the hole acceptors taking into consideration only the increase in the efficiency of the removal of the photogenerated holes and stated that the dissolved substances hinder photoanodic oxygen formation on the electrode surface, thereby sharply reducing the effect of recombination via photoelectrochemical reaction products which is essentially characteristic of nanostructured electrodes.

Compared with compact polycrystalline and single-crystal electrodes, porous nanocrystalline TiO_2 films considerably have a stronger dependence of their photoelectrochemical properties on the presence of electron and hole acceptors in solution [45].

The depletion of the photocurrent signal is inversely proportional to the concentration of oxidizable species; but, for film thicknesses in the range of 1–2 μm or above, this effect is superimposed by the relatively slow response to irradiation [34]. This photocurrent depletion has been postulated [31] as being due to a depletion of the Helmholtz layer in oxalate after an initial current spike; therefore, the oxidation of water and the electron–hole recombination become more probable, thus decreasing the probability of electrons reaching the back contact.

Notwithstanding the enhanced photocurrent, dark-light periods in the presence of oxalate seem to affect the final response: the shape of the photocurrent decay does not present a constant behavior in all the transients used for the quantification of the time constant, thus not allowing a reliable elaboration of the data. Moreover, considering that oxalate as a hole scavenger prevents the electron–hole recombination and that there are different oxalate adsorption phenomena on the oxides samples depending on the specific surface areas (3rd column of Table 1); we consequently decided to perform comparison among the samples without the presence of oxalate in solution and found that, indeed, these factors could affect the evaluation of the intrinsic charge recombination properties of each sample.

3.2 Role of the illumination source

Figure 4 compares the photocurrent recorded on T sample under UV or visible irradiation. The higher photocurrent obtained when using UV light could be attributed to extra photogenerated charge carriers at the semiconductor/electrolyte interface, which would even result in the increase of the electric field produced in the depletion layer in case of bigger semiconductor particles. Moreover, in the case of UV irradiation, the photocurrent decay is steeper, probably because the electronic levels involved are different from those populated by visible light excitation. However, the trend of the transient time constants obtained for a set of samples is maintained when using the two types of irradiation sources. The emission spectra have been reported in Fig. 4b.

3.3 Doped TiO_2 electrodes

In order to properly characterize doped TiO_2 samples which exhibit a marked absorption in the visible region (Fig. 5), possibly due to intra-gap states (see related

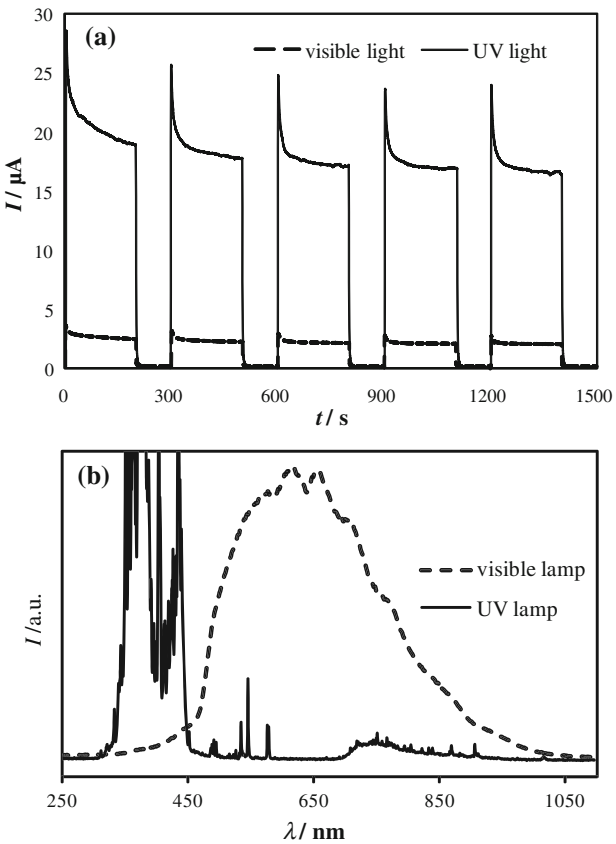

Fig. 4 Example of photocurrent transients recorded under UV or visible light (**a**); emission spectrum of the two lamps employed during electrochemical measurements (**b**)

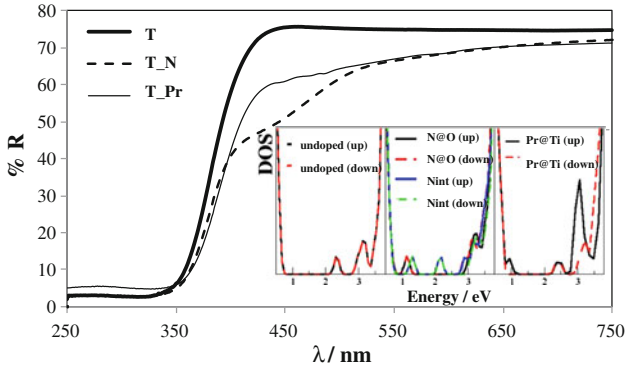

Fig. 5 Diffuse reflectance spectra of all samples. *Inset*: electronic DOS obtained by planewave DFT calculations for undoped (*left*) N-doped (*center*) and Pr-doped TiO_2 (*right*), for both spin up and spin down configurations. Symbol "@" indicates a substitutional position for the dopant and "Nint" refers to interstitial N

computed DOS in inset) leading to a shrinking of the apparent band gap (Table 1, 8th column), visible light photocurrent measurements have been recorded.

The main morphological, structural, and optical features of the samples under study are summarized in Table 1. While Pr-TiO_2 samples show lower surface areas and pore volumes than N-TiO_2 ones, both dopants lead to titania with similar phase composition (anatase as main polymorph and brookite as the secondary one). The crystallite size is only slightly higher for T_Pr. The high-resolution transmission electron micrographs presented in Fig. 6 show some tendency of agglomeration for the N-doped sample and, for both dopants, well-crystallized domains and more prismatic particles than the spherical ones observed in the case of the pristine oxide.

The effect of doping on charge carriers' recombination can be considered twofold: it is said to be detrimental due to the introduction of sites in the lattice—or electronic levels in the band gap—that accelerate the rate of electron–hole recombination, or positive, owing to the creation of sites which can selectively trap charge carriers. As a final balance, it depends on the position of electronic levels introduced by doping in the band gap, on the amount of doping, on the photocatalytic reaction, and on several other factors involved in it [44, 51].

By analyzing each photocurrent transient (Fig. 7a), a less steep decay is obtained for our N-doped and Pr-doped samples; as derived by the normalized plot of current–time dependence (Fig 7b), we found that both doped oxides show a higher τ, thus a slower recombination rate, than the undoped one (see the numerical values in the inset table of Fig. 7b).

By performing time-resolved laser flash photolysis on colloidal aqueous TiO_2 suspensions, Bahnemann et al. [52] showed that deeply trapped holes (i.e., surface-bound hydroxyl radicals) are rather long-lived and unreactive,

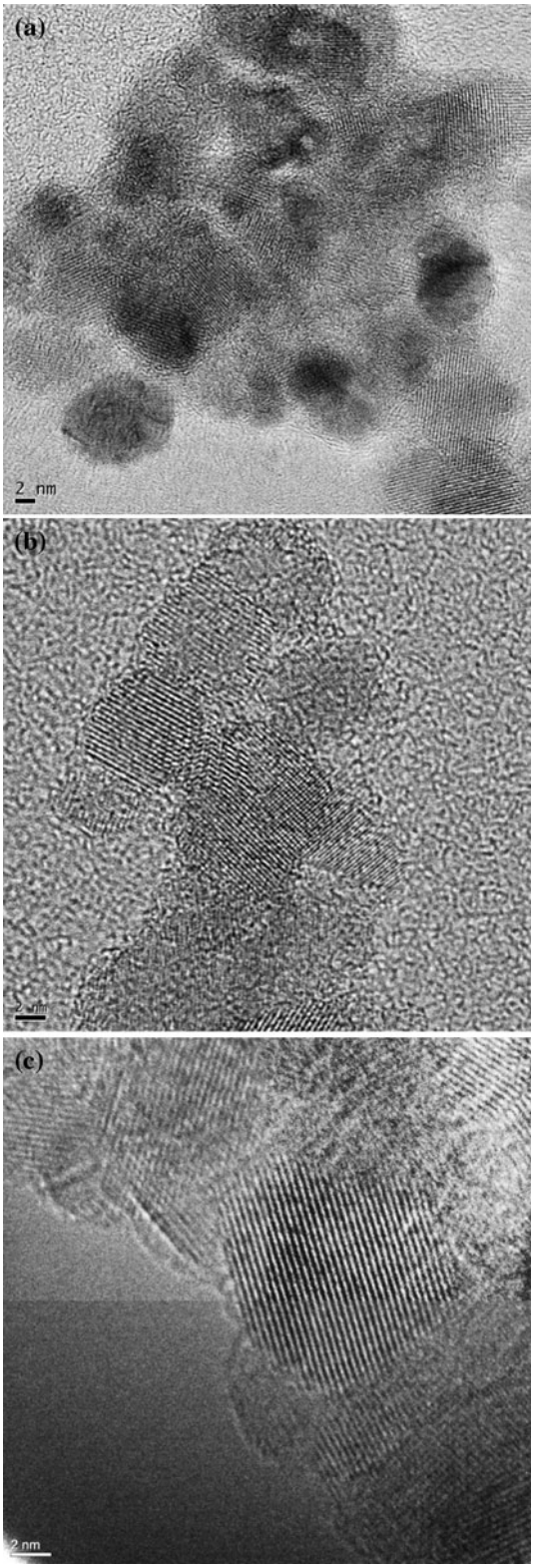

Fig. 6 HR-TEM images of doped and undoped titania samples: T (**a**), T_N (**b**), T_Pr (**c**)

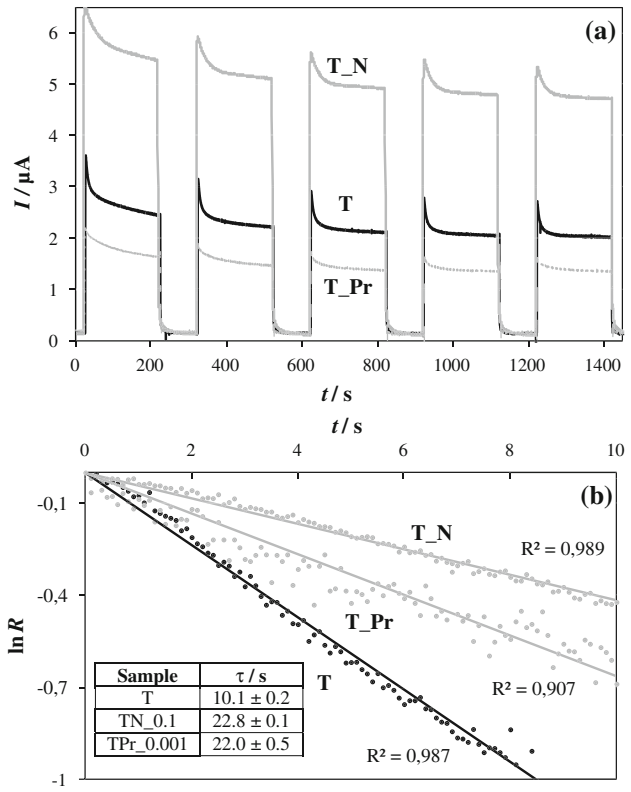

Fig. 7 Comparison of photocurrent transients for doped and undoped titania samples (**a**); normalized plot of current–time dependence for the same samples with the *inset* table showing their transient time constants (**b**)

while shallowly trapped holes are in a thermally activated equilibrium with free holes and exhibit a very high oxidation potential.

Further, according to Grabtchak et al.[53], much of the information on the form of the density of states over an energy range of up to 0.5 eV depth is contained in the detailed form of the initial decay of the photocurrent on a timescale $<10^{-10}$ s in which only the shallowest traps are expected to have an effect. Our time scale is definitely larger so that all types of electrons/holes traps can be active.

4 Conclusions

The use of photocurrent measurements for the characterization of semiconductor thin film electrodes could be not straightforward due to the lack of a widely accepted experimental procedure and the several parameters involved in this type of analysis (layer reproducibility, choice of extrapolation time range, photoanode modification during analysis, etc.).

In this paper, an optimization of experimental parameters, to achieve a reliable insight into the relation between the type/concentration of a dopant and charge carriers recombination rate, was performed.

Optimal parameters have proved to consist in the use of an aqueous inert electrolyte (0.1 M $NaClO_4$) in a nitrogen-purged cell. Furthermore, a proper applied potential (+1.0 V vs SCE) was chosen by recording linear sweep voltammetries and a long dark equilibration time (600 s) was used to reach equilibrium in the dark. These conditions were successfully applied for the characterization of selected doped samples and seem a viable and fast route to investigate the dynamics of charge carriers in a thin films, either under visible or UV illumination.

With this optimized method, suitable conditions to compare doped and undoped TiO_2 powders, deposited as films, which showed different morphological features (i.e., specific surface areas and pore volumes in the range of 95–170 $m^2\ g^{-1}$ and 0.10–0.31 mL g^{-1}, respectively), were designed.

Further investigations will involve the screening of several other doped samples to evaluate the influence of different synthetic conditions on the recombination rate.

References

1. Nissfolk J, Fredin K, Simiyu J, Häggman L, Hagfeldt A, Boschloo G (2010) J Electroanal Chem 646:91–99
2. Buonsanti R, Carlino E, Giannini C, Altamura D, De Marco L, Giannuzzi R, Manca M, Gigli G, Cozzoli PD (2011) J Am Chem Soc 133:19216–19239
3. McGehee MD (2011) Science 334:607–608
4. O'Regan B, Grätzel M (1991) Nature 353:737–740
5. Nazeeruddin MK, Kay A, Rodicio I, Humphrey-Baker R, Mueller E, Liska P, Vlachopoulos N, Grätzel M (1993) J Am Chem Soc 115:6382–6390
6. Hagfeldt A, Vlachopoulos N, Grätzel M (1994) J Electrochem Soc 141:82–84
7. Vinodgopal K, Hotchandani S, Kamat PV (1993) J Phys Chem 97:9040–9044
8. Hagfeldt A, Grätzel M (1995) Chem Rev 95:49–68
9. Könenkamp R, Henniger R, Hoyer P (1993) J Phys Chem 97:7328–7330
10. Kay A, Humphry-Baker R, Grätzel M (1994) J Phys Chem 98:952–959
11. Hoyer P, Eichberger R, Weller H Ber. Bunsenges (1993) Phys Chem 97:630–635
12. Hoyer P, Weller H (1995) J Phys Chem 99:14096–14100
13. Benkstein KD, Kopidakis N, Van de Lagemaat J, Frank AJ (2003) J Phys Chem B 107:7759–7767
14. Cass MJ, Walker AB, Martinez D, Peter LM (2005) J Phys Chem B 109:5100–5107
15. Fredin K, Ruhle S, Grasso C, Hagfeldt A (2006) Sol Energy Mater Sol Cells 90:1915–1917
16. Kopidakis N, Schiff EA, Park NG, Van de Lagemaat J, Frank AJ (2000) J Phys Chem B 104:3930–3936
17. Cao F, Oskam G, Searson PC (1996) J Phys Chem 100:17021–17027
18. Dloczik L, Ileperuma O, Lauermann I, Peter L, Ponomarev E, Redmond G, Shaw N, Uhlendorf I (1997) J Phys Chem B 101:10281–10289

19. De Jongh PE, Vanmaekelbergh D (1997) J Phys Chem B 101:2716–2722
20. Schlichthörl G, Park NG, Frank AJ (1999) J Phys Chem B 103:782–791
21. Solbrand A, Lindström H, Rensmo H, Hagfeldt A, Lindquist S-E, Södergren S (1997) J Phys Chem B 101:2514–2518
22. Fabregat-Santiago F, Bisquert J, Garcia-Belmonte G, Boschloo G, Hagfeldt A (2005) Sol Energy Mater Sol Cells 87:117–131
23. Wang Q, Ito S, Grätzel M, Fabregat-Santiago F, Mora-Sero I, Bisquert J, Bessho T, Imai H (2006) J Phys Chem B 110: 25210–25221
24. O'Regan BC, Bakker K, Kroeze J, Smit H, Sommeling P, Durrant JR (2006) J Phys Chem B 110:17155–17160
25. Greijer-Agrell H, Boschloo G, Hagfeldt A (2004) J Phys Chem B 108:12388–12396
26. Kroeze JE, Savenije TJ, Warman JM (2004) J Am Chem Soc 126:7608–7618
27. Hendry E, Koeberg M, O'Regan B, Bonn M (2006) Nano Lett 6:755–759
28. Boschloo GK, Goossens A (1996) J Phys Chem 100:19489–19494
29. Lee G-W, Bang S-Y, Lee C, Kim W-M, Kim D, Kim K, Park N-G (2009) Curr Appl Phys 9:900–906
30. Taffa DH, Kathiresan M, Arnold T, Walder L, Erbacher M, Bauer D, Montforts F-P, Nordmann J, Haase M (2010) J Photochem Photobiol A Chem 216(2010):35–43
31. Byrne JA, Eggins BR (1998) J Electroanal Chem 457:61–72
32. Zheng J, Yu H, Li X, Zhang S (2008) Appl Surf Sci 254: 1630–1635
33. Zhang W-D, Jiang L-C, Ye J-S (2009) J Phys Chem C 113:16247–16253
34. Waldner G, Krýsa J, Jirkovský J, Grabner G (2003) Int J Photoenergy 5:115–122
35. Krýsa J, Zlamal M, Waldner G (2007) J Appl Electrochem 37:1313–1319
36. Goossens A, Van der Zanden B, Schoonman J (2000) Chem Phys Lett 331:1–6
37. Spadavecchia F, Cappelletti G, Ardizzone S, Bianchi CL, Cappelli S, Oliva C, Scardi P, Leoni M, Fermo P (2010) Appl Catal B Environ 96:314–322
38. Kresse G, Hafner J (1996) Phys Rev B 47:558–561
39. Kresse G, Joubert D (1999) Phys Rev B 59:1758–1775
40. Meroni D, Ardizzone S, Cappelletti G, Oliva C, Ceotto M, Poelman D, Poelman H (2009) Catal Today 161:169–174
41. Spadavecchia F, Cappelletti G, Ardizzone S, Ceotto M, Falciola L (2011) J Phys Chem C 115:6381–6391
42. Hagfeldt A, Lindström H, Södergren S, Linquist S-E (1995) J Electroanal Chem 381:39–46
43. Chuang H-Y, Chen Int D-H (2011) J Hydrogen Energy 36: 9487–9495
44. Wang H, He J, Boschloo G, Lindström H, Hagfeldt A, Lindquist S-E (2001) J Phys Chem B 105:2529–2533
45. Poznyak SK, Kokorin AI, Kulak AI (1998) J Electroanal Chem 442:99–105
46. Dholam R, Patel N, Santini A, Miotello A (2010) Int J Hydrogen Energy 35:9581–9590
47. Tafalla D, Salvador P, Benito RM (1990) J Electrochem Soc 137:1810–1815
48. Rensmo H, Lindstrom H, Södergren S, Willstedt A, Solbrand A, Hagfeldt A, Lindquist S-E (1996) J Electrochem Soc 143:3173–3178
49. Xiao S, Qu J, Liu H, Zhao X, Wan D (2009) J Solid State Electrochem 13:1959–1964
50. Zanoni MVB, Sene JJ, Selcuk H, Anderson MA (2004) Environ Sci Technol 38:3203–3208
51. Radecka M, Rekas M, Trenczek-Zajac A, Zakrzewska K (2008) J Power Sources 181:46–55
52. Bahnemann DW, Hilgendorff M, Memming R (1997) J Phys Chem B 101:4265–4275
53. Grabtchak S, Main C, Reynolds S (2000) J Non-Crys Sol 266–269:362–366